Toxicology and Applied Pharmacology 269 (2013) 250–262

Contents lists available at SciVerse ScienceDirect

Toxicology and Applied Pharmacology

journal homepage: www.elsevier.com/locate/ytaap

Pulmonary instillation of low doses of titanium dioxide nanoparticles in mice leads to particle retention and gene expression changes in the absence of inflammation

Mainul Husain [a], Anne T. Saber [b], Charles Guo [a], Nicklas R. Jacobsen [b], Keld A. Jensen [b], Carole L. Yauk [a], Andrew Williams [b], Ulla Vogel [b,c], Hakan Wallin [b,d], Sabina Halappanavar [a,*]

[a] Environmental Health Science and Research Bureau, Health Canada, Ottawa, Ontario K1A 0K9, Canada
[b] The Danish NanoSafety Centre, National Research Centre for the Working Environment, Copenhagen DK-2100, Denmark
[c] Department of Micro- and Nanotechnology, Technical University of Denmark, Kgs. Lyngby DK-2800, Denmark
[d] Institute of Public Health, University of Copenhagen, Copenhagen DK-1014, Denmark

ARTICLE INFO

Article history:
Received 23 January 2013
Revised 11 March 2013
Accepted 21 March 2013
Available online 1 April 2013

Keywords:
Hyperspectral microscopy
Gene expression
Inflammation
Muscle contraction
Calcium homeostasis
Tissue particle retention

ABSTRACT

We investigated gene expression, protein synthesis, and particle retention in mouse lungs following intratracheal instillation of varying doses of nano-sized titanium dioxide (nano-TiO_2). Female C57BL/6 mice were exposed to rutile nano-TiO_2 via single intratracheal instillations of 18, 54, and 162 μg/mouse. Mice were sampled 1, 3, and 28 days post-exposure. The deposition of nano-TiO_2 in the lungs was assessed using nanoscale hyperspectral microscopy. Biological responses in the pulmonary system were analyzed using DNA microarrays, pathway-specific real-time RT-PCR (qPCR), gene-specific qPCR arrays, and tissue protein ELISA. Hyperspectral mapping showed dose-dependent retention of nano-TiO_2 in the lungs up to 28 days post-instillation. DNA microarray analysis revealed approximately 3000 genes that were altered across all treatment groups (±1.3 fold; $p < 0.1$). Several inflammatory mediators changed in a dose- and time-dependent manner at both the mRNA and protein level. Although no influx of neutrophils was detected at the low dose, changes in the expression of several genes and proteins associated with inflammation were observed. Resolving inflammation at the medium dose, and lack of neutrophil influx in the lung fluid at the low dose, were associated with down-regulation of genes involved in ion homeostasis and muscle regulation. Our gene expression results imply that retention of nano-TiO_2 in the absence of inflammation over time may potentially perturb calcium and ion homeostasis, and affect smooth muscle activities.

Introduction

Titanium dioxide (TiO_2) is generally considered to be chemically inert because it is highly insoluble, thermally stable, and non-flammable. However, rats exposed to high doses of pigment-grade and ultrafine TiO_2 dust by inhalation or instillation develop lung cancer (Heinrich et al., 1995). In addition, the International Agency for Research on Cancer has classified pigment-grade TiO_2 (microparticles with size range of 100–200 nm) as a possible human carcinogen (group 2B) (IARC, 2010; Iavicoli et al., 2011) based on animal and cell culture data, but there is little evidence for TiO_2-mediated carcinogenic effects in humans. TiO_2 is produced primarily as aggregates or agglomerates of nano-sized particles. It accounts for 70% of the total production of pigments worldwide. TiO_2-nanoparticles (TiO_2-NPs) are extensively used in a wide range of products including paints, coatings, cosmetics, and sunscreens (Liao et al., 2008; Madl and Pinkerton, 2009; Park et al., 2009). As a result of the high production volume and extensive applications of powdered TiO_2, reasonable risks for exposures through inhalation or via other routes are anticipated. TiO_2-NPs exhibit unique physico-chemical properties associated with their nano-size, which alters their biological behaviors at the cellular, subcellular, and protein levels resulting in adverse health effects (Liu et al., 2009; Nemmar et al., 2011; Oberdorster et al., 2000; Warheit et al., 2007). Thus, a detailed characterization of the tissue-level effects and mechanisms of action of TiO_2-NPs is required in order to establish acceptable exposure limits.

Lung is a primary target organ of NP exposure via inhalation in occupational settings. Pulmonary responses are largely driven by the physico-chemical properties of the NPs, and it is well established that inhalation of TiO_2-NPs induces pulmonary responses that primarily include inflammation. Ferin et al. (1992) were the first to demonstrate that pulmonary responses in rats exposed to TiO_2-NPs are greatly influenced by particle size (Ferin et al., 1992). These authors also showed that intratracheal instillation or inhalation of TiO_2-NPs induces profound neutrophilic inflammation/infiltration, translocation of particles to the deeper regions of lungs, and longer retention of particles compared to their microparticulate counterpart. Similar particle size-associated effects

* Corresponding author at: Environmental Health Science and Research Bureau, ERHSD, HECSB, Health Canada, Tunney's Pasture, Bldg. 8 (P/L 0803A), 50 Columbine Driveway, Ottawa, Ontario K1A 0K9, Canada. Fax: +1 613 941 8530.
E-mail addresses: mainul.husain@hc-sc.gc.ca (M. Husain), ats@nrcwe.dk (A.T. Saber), charles.guo@hc-sc.gc.ca (C. Guo), nrj@nrcwe.dk (N.R. Jacobsen), kaj@nrcwe.dk (K.A. Jensen), carole.yauk@hc-sc.gc.ca (C.L. Yauk), andrew.williams@hc-sc.gc.ca (A. Williams), ubv@nrcwe.dk (U. Vogel), hwa@nrcwe.dk (H. Wallin), sabina.halappanavar@hc-sc.gc.ca (S. Halappanavar).

0041-008X
http://dx.doi.org/10.1016/j.taap.2013.03.018

on pulmonary inflammation in rats were also observed by Renwick et al. (2004). Additional evidence suggests that the adverse pulmonary effects associated with TiO_2-NPs are further amplified if the NPs are surface-coated with alumina or amorphous silica (Warheit et al., 2007). Inflammatory response to TiO_2-NPs varies depending on the crystalline form (Grassian et al., 2007), with mixed rutile/anatase forms exhibiting increased toxicity over other types of TiO_2-NPs driven by the larger surface areas of mixed TiO_2-NP types (Warheit et al., 2007). Thus, these and other studies (reviewed in (Johnston et al., 2009)) firmly establish that TiO_2-NPs elicit pulmonary toxicity and tissue injury, and that the toxicity is based on several physical and chemical properties.

Several studies have shown that ultrafine particles or NPs effectively evade primary phagocyte-mediated clearance mechanisms in the lungs and hence migrate to the deeper interstitial regions of the lungs where they are retained over long periods of time (Ferin et al., 1992; Katsnelson et al., 2010). Other studies have suggested that excessive pulmonary retention and accumulation of particles may lead to lung injury and/or enhanced risks of developing cancer (Bermudez et al., 2002, 2004; Heinrich et al., 1995). However, most of these studies used physiologically irrelevant doses and thus, the biological implication of low dose exposure to TiO_2-NPs, and the underlying molecular mechanisms of the observed pulmonary responses, remain largely unknown. Additionally, very few studies have examined the effects of retained particles following low dose exposures on pulmonary systems.

We (Saber et al., 2012) recently compared pulmonary response in mice following single instillation doses of 18, 54 and 162 μg of nano-TiO_2/mouse, corresponding to 1.5, 5 and 15 working days at the Danish occupational exposure level for TiO_2 (6.0 mg Ti/m^3–9.75 mg TiO_2/m^3) at three different post-exposure time points, and showed dose- and time-dependent pulmonary neutrophilic inflammation. Interestingly, the lowest dose in this study did not elicit any pulmonary inflammation as measured by inflammatory cellular influx in the bronchoalveolar lavage fluid (BAL). Based on these results a No Observed Effect Level (NOEL) for nano-TiO_2 of 19 cm^2 was derived for mice, corresponding to the lowest tested dose (Saber et al., 2012).

It could be hypothesized that the lack of inflammatory cell influx in the BAL at the low doses observed in the study described above is a result of first-order rates of clearance in the low dose range. In the present study we rationalized that the lack of observable changes in inflammatory cell influx reported by Saber et al. (2012), is actually the result of diminished induction of clearance mechanisms at low dose NP exposures, and that NPs will thus still be present in the lungs even in the absence of inflammation. To test our hypothesis we used nanoscale hyperspectral microscopy to measure nano-TiO_2 retention in the lungs of the same mice used by Saber et al. (2012), in parallel with pulmonary gene and protein expression profiling, to study dose and time-related responses. We expected to find significant retention of particles in lungs at all doses over extended periods of time resulting in perturbations of normal biological functions. An additional objective for this study was to generate testable hypotheses for novel mechanisms involved in pulmonary effects induced by low doses of nano-TiO_2.

Materials and methods

The experimental samples used in this study were generated in an earlier study; the animals, characterization of particles, exposure, and exposure monitoring are previously described in Saber et al. (2012) and are briefly outlined below.

Animals

Five-to-seven week old female C57BL/6 mice were purchased from Taconic (Ry, Denmark) and were acclimatized for 1–3 weeks prior to the commencement of the experiment. Mice were maintained in groups in polypropylene cages with sawdust bedding and enrichment, at 20–22 °C room temperature and relative humidity of 40–60% with a 12 h light-to-dark cycle. All mice received food and water ad libitum throughout the experiment. All animal experiments were approved by the Danish "Animal Experiments Inspectorate" and performed according to their guidelines for ethical conduct in the care and use of animals in research.

Particle characterization and preparation of exposure stock

The nanomaterial used in this study was an ultrafine powder of surface coated rutile TiO_2 also known as UV-Titan L181 (Kemira, Pori, Finland) with an average crystallite size of 20.6 nm and surface area of 107.7 m^2/g, and is termed 'nano-TiO_2' throughout this article. Details of the particle characterization were described previously (Halappanavar et al., 2011; Hougaard et al., 2010), and are summarized in Table 1.

Naïve C57BL/6 mice were flushed twice with 0.6 ml of 0.9% NaCl to obtain approximately 1 ml of bronchoalveolar lavage fluid (BAL). BAL was centrifuged at 400 *g* for 10 min at 4 °C to remove cells. The supernatant was used in the dispersant liquid. A total of 4.05 mg of nano-TiO_2 was suspended in 1 ml of MilliQ water containing 0.9% NaCl and 10% v/v acellular BAL. Particle suspensions were prepared by sonicating the samples using an S-450D sonifier (Branson Ultrasonics Corp., Danbury, CT, USA) at 10% amplitude for a total of 16 min on ice with alternating 10 s pulses and pauses. Three different dilutions of nano-TiO_2 were prepared and used in this experiment: 162 μg, 54 μg (1:3 dilution of the 162 μg), and 18 μg (1:3 dilution of the 54 μg). Control vehicle solutions were prepared without the nano-TiO_2 (MilliQ water containing 90% of 0.9% NaCl and 10% acellular BAL fluid). The doses 18, 54, and 162 μg/mouse are equivalent to 1.5, 5, and 15 working days at the Danish occupational exposure level for TiO_2 (6.0 mg Ti/m^3–9.75 mg TiO_2/m^3), respectively (Saber et al., 2012).

Exposure of mice and harvesting of tissue

Each treatment group consisted of a minimum of 6 animals. Mice in the experimental groups received a single intratracheal instillation of 18 (low dose), 54 (medium dose), or 162 μg (high dose) of nano-TiO_2 in a 40 μl suspension as described above, followed by 150 μl air with a 250 μl SGE glass syringe (250F-LT-GT, MicroLab, Aarhus, Denmark). Intratracheal instillation was performed at 37 °C on heating plates, under anesthesia using Hypnorm® (fentanyl citrate 0.315 mg/ml and fluanisone 10 mg/ml from Janssen Pharma) and Dormicum® (Midazolam 5 mg/ml from Roche). Control mice received 40 μl of dispersant vehicle only. Following instillation, mice were under observation until they recovered from anesthesia. Mice were allowed to recover for

Table 1
Physical and chemical characteristics of nano-TiO_2 (modified from Halappanavar et al., 2011; Hougaard et al., 2010).

Description	Composition
Phase	Rutile
Form	Powder
Structural formula	Ti_2O_4
Average crystalline size	20.6 ± 0.3 nm
Minimum crystalline size [100][a]	14.4–15.5 nm
Maximum crystalline size [001][a]	38.4 nm
Specific surface area	107.7 m2/g
Elements	Content [wt%]
Silicon	5.61
Titanium	42.44
Aluminum	2.42
Zirconium	0.86
Sodium	0.45
Oxygen[b]	35.24
Coating	Silicon, aluminum, zirconium and polyalcohol

[a] Estimate of the average crystalline size along the shortest and longest crystallographic direction.
[b] Calculated by difference from 100 wt.%.

24 h, 3 days, and 28 days following instillation before being euthanized under anesthesia (Hypnorm/Dormicum). Blood, BAL fluid, and tissues were collected. Lung tissues from experimental and control mice were cut into small pieces, stored in cryogenic vials, and snap frozen immediately in liquid nitrogen. All tissues were stored at −80 °C until analysis. All analyses including microarray, validation of microarray results, protein analysis, and microscopic imaging for detection of particles were conducted on the left lobe of the lung tissue.

Detection of nano-TiO_2 in lung tissue

Frozen lung tissue samples (n = 2–3) from low and medium dose groups sampled on day 1 and day 28 and matched controls were embedded in paraffin. Paraffin-embedded tissues were sliced into 5 μm thick sections and stained with hematoxylin-eosin (H-E). H-E stained lung tissue sections (two sections per sample) were sent to CytoViva, Inc. (Auburn, AL, USA) for hyperspectral imaging and quantitative mapping of nano-TiO_2 particles in the lungs. The proprietary hyperspectral imaging technology uses a nano-scale microscope and a darkfield-based optical illuminator to focus light on samples, yielding images with improved contrast and signal-to-noise ratio. Such imaging technique takes advantage of the intrinsic light scattering properties of the particle of interest (e.g., nano-TiO_2 particles). The hyperspectral imager consists of a concentric imaging visible and near-infrared (VNIR) spectrophotometer (400–1000 nm) with integrated CCD camera, and is controlled by Environment for Visualization (ENVI 4.8) software for hyperspectral image analysis. The images (100× magnification) were captured using a Dage Excel Color Cooled-M camera that is attached to an Olympus BX 43 optical microscope. In order to aid the identification and image analysis process, a reference spectral library of nano-TiO_2 was created prior to the analysis of the actual sample images using a customized software analysis program, and coded experimental samples were compared to those in the reference library. Samples were decoded after the completion of analysis to examine particle-related retention.

Total RNA extraction and purification

The total tissue for RNA extraction varied between 10 and 15 mg from each animal. In order to ensure unbiased analysis of tissue response, total RNA was isolated from randomly sectioned (weighing 10–15 mg) left lung lobe. RNA was isolated from 5 to 6 individual animals from each of the treatment and control groups using TRIzol reagent (Invitrogen, Carlsbad, CA, USA) and purified using RNeasy Plus Mini kits (Qiagen, Mississauga, ON, Canada) according to the manufacturer's instruction. Total RNA concentration was measured using a NanoDrop 2000 spectrophotometer (Thermo Fisher Scientific Inc., Wilmington, DE, USA), and RNA quality and integrity were assessed using an Agilent 2100 Bioanalyzer (Agilent Technologies, Inc., Mississauga, ON, Canada) according to the manufacturer's instruction. All samples showed RNA integrity numbers of 7 and above, indicating high quality RNA, and were used to conduct microarray and qPCR experiments.

Microarray hybridization

Total RNA (250 ng) samples from individual mice (n = 5–6 per experimental and control group) and from universal reference total RNA (Agilent Technologies, Inc., Mississauga, ON, Canada) were used to synthesize double-stranded cDNA and cyanine labeled cRNA using Quick Amp Labeling Kit (Agilent Technologies Inc., Mississauga, ON, Canada) according to the manufacturer's instructions. Control and nano-TiO_2 treated cRNAs were labeled with cyanine 5-CTP, and reference RNAs were labeled with cyanine 3-CTP using a T7 RNA polymerase in vitro transcription kit (Agilent Technologies Inc., Mississauga, ON, Canada) and purified using RNeasy Mini kits (Qiagen, Mississauga, ON, Canada). Each experimental cRNA sample was mixed with an equimolar amount of reference cRNA and was hybridized to Agilent mouse 4 × 44 oligonucleotide microarrays (Agilent Technologies Inc., Mississauga, ON, Canada) for 17 h in a hybridization chamber at 65 °C with a rotation speed of 10 rpm. Arrays were washed according to manufacturer's protocols (Agilent Technologies Inc., Mississauga, ON, Canada) and scanned on an Agilent G2505B scanner. Data from the scanned images were extracted using Agilent Feature Extraction software version 9.5.3.1. All microarray data from this study are available at the National Center for Biotechnology Information (NCBI) and Gene Expression Omnibus (GEO) databases. GEO accession number for these files is GSE41041.

Statistical analysis of microarray data

A reference randomized block design (Kerr, 2003; Kerr and Churchill, 2007) was used to analyze gene expression microarray data. Data were normalized using *LO*cally *W*Eighted *S*catterplot *S*moothing (LOWESS) (Cleveland, 1979) regression modeling method and statistical significance of the differentially expressed genes was determined using *M*icro*A*rray *AN*alysis *O*f *VA*riance (MAANOVA) (Wu et al., 2003) in R statistical software (http://www.r-project.org). The Fs statistic (Cui et al., 2005) was used to test the treatment effects and *p*-values were estimated by the permutation method using residual shuffling. The false discovery rate (FDR) multiple testing correction (Benjamini and Hochberg, 1995) was applied to minimize any false positives. Fold change calculations were based on the least-square means. Genes showing expression changes of at least 1.3 fold in either direction compared to their matched controls and having *p*-values of less than or equal to 0.1 ($p \leq 0.1$) were considered as significantly differentially expressed and were used in the downstream analysis. We applied a liberal approach since we were looking for effects in the low dose range in the absence of any observable phenotype.

Functional and pathway analysis of differentially expressed genes

Functional gene ontology (GO) analysis of the differentially expressed genes was performed using the Database for Annotation, Visualization and Integrated Discovery (DAVID) v6.7 (Huang da et al., 2009). Benjamini–Hochberg corrected GO processes with a Fisher's exact $p \leq 0.05$ were considered to be significantly enriched (over-represented). Specific biological pathways associated with the differentially expressed genes were identified using Ingenuity Pathway Analysis (IPA, Ingenuity Systems, Redwood City, CA, USA) and MetaCore (Thomson Reuters Scientific Inc., Philadelphia, PA, USA) software. Pathways with a Fisher's exact *p*-value of ≤0.05 ($p \leq 0.05$) were considered for discussion. The pathway analysis methods employed in the present study enable the extraction of biologically meaningful information from a long list of differentially expressed genes. The quality and annotation of different pathway analysis packages vary. Therefore, the methods employed in our study are considered a starting point, and are used to direct future research. For a detailed review on the limitations of the present pathway analysis approaches please refer to Khatri et al. (2012).

Real-time PCR (qPCR) validation of microarray data

Mouse inflammatory cytokines and receptors (PAMM-011A, SABiosciences, Frederick, MD, USA) and custom PCR arrays were used to validate 126 genes in total. Genes for the custom PCR array (CAPM11274, SABiosciences, Frederick, MD, USA) were selected based on their established roles in biological processes such as acute phase response, ion homeostasis, lipid metabolism, and muscle regulation, and exhibited fold changes of at least ±1.3 ($p \leq 0.1$). Approximately 800 ng of the total RNA (n = 3 per group) from each of the experimental and control groups of mice was reverse transcribed using an RT^2 first strand cDNA synthesis kit (SABiosciences, Frederick, MD, USA). qPCRs were conducted using RT^2 SYBR Green qPCR Master Mix in a CFX96 Real-Time System (BioRad Laboratories, Mississauga, ON, Canada) according to the manufacturer's instructions. Threshold cycle (Ct) values

were normalized using *Hprt*, *Hsp90ab1*, and *Gapdh* as internal control genes, and relative expression of the differentially expressed genes was determined using online PCR array data analysis software (SABiosciences, Frederick, MD, USA). The correlation between the qPCR and microarray fold changes of the validated genes was determined using Spearman's rank correlation analysis (Spearman, 1904) in R statistical software. A Shapiro–Wilk normality test (Shapiro and Wilk, 1965) for the fold change datasets was performed prior to the correlation analysis to identify if the data were normally distributed.

Expression analysis of inflammatory proteins

Total protein from the frozen lung tissues ($n = 3$) from experimental and control mice was extracted using Bio-Plex Cell Lysis Kits (BioRad Laboratories, Mississauga, ON, Canada) and quantified using Bradford protein assay kits (Bio-Rad Laboratories, Mississauga, ON, Canada). Expression of mouse pro-inflammatory cytokines was assessed using Pro Mouse Cytokine 23-plex and 9-plex assay kits (BioRad Laboratories, Mississauga, ON, Canada) according to the manufacturer's instructions in a Bio-Plex 200 system (BioRad Laboratories, Mississauga, ON, Canada). Briefly, 100 μg of each lysate was diluted with the manufacturer supplied sample diluents. Anti-cytokine/chemokine antibody-conjugated magnetic beads were immobilized in each individual well of the 96 well filter plates using a vacuum manifold. Plates were washed twice, and 50 μl of pre-diluted standards and sample lysates was added to each of the designated well. Plates were shaken at room temperature for 30 min at 350 rpm. Following 3 washes, plates were incubated for 30 min with 25 μl of pre-diluted multiplex detection antibody. Plates were washed 3 times and incubated with 50 μl of pre-diluted streptavidin-conjugated phycoerythrin for 10 min. Following a final 3-step wash, plates were incubated with 125 μl of assay buffer in each well and were analyzed using the Bio-Plex protein assay system. The concentration of each cytokine and chemokine was determined using Bio-Plex Manager Version 6.0 software.

Results

The pulmonary inflammatory response was assessed to investigate the impact of nano-TiO_2 deposition in mouse lungs by measuring BAL differential cell counts and the results were published (Saber et al., 2012). Since the inflammatory phenotype reported in Saber et al. (2012) provides context to the present study, the results are summarized below. Briefly, exposure to nano-TiO_2 induced a significant inflammatory response in the 54 μg dose group on days 1 and 3, and in the 162 μg dose group across all the post-exposure time points studied. Inflammation was mainly characterized by an increase in the total cellular count and inflammatory neutrophils in BAL. Inflammation was pronounced on day 1 for both of these dose groups and was partially resolved by 28 days post-exposure time. No significant changes were observed in the BAL cellular profiles of the 18 μg dose group compared to the controls.

Detection of nano-TiO_2 in lung tissue

In order to understand if lack of inflammation in the low dose group is attributed to the efficient clearance of particles, the lungs of mice exposed to low (18 μg) or high (162 μg) doses of nano-TiO_2 sampled on days 1 and 28 post-exposure were examined for particle retention using the CytoViva patented VNIR hyperspectral imaging system and darkfield microscopy. Nanoparticles in general have a significantly different refractive index from the surrounding tissue, stains, and mounting medium used to process the tissues, which leads to greater scattering of light in the sections containing NPs and hence their easy detection. Two reference spectral libraries were made. The first library established a complete spectral profile of the nano-TiO_2 used in this study (Fig. 1a). The second library cataloged a set of bright non-specific inclusions that were fluorescing as strongly as the nano-TiO_2, but were also found in the untreated control samples (Fig. 1b). These non-specific inclusions are the result of endogenous cellular materials fluorescing in all samples. Images from the treated samples were overlaid with the reference spectral library for nano-TiO_2 for accurate and precise detection of nano-TiO_2 particles in the exposed samples.

Fig. 1c shows dark field (upper panel), dark field hyperspectral (middle panel), and hyperspectral mapping (bottom panel, overlay of dark field hyperspectral images with nano-TiO_2 reference spectra) images. Qualitative analysis of particle-laid lung tissues showed aggregated and agglomerated nano-TiO_2 (white inclusions indicated by white arrow heads) in random parts of the lung tissue increasing in a dose-dependent manner. A significant amount of nano-TiO_2 was observed in day 1 as well as in day 28 post-exposure samples (Fig. 1c, upper panel). We did not apply a quantitative approach to measure the exact numbers of particles or aggregates. Quantitative analyses would require highly precise localized sectioning to compare the exact same lung regions across the samples, which was not possible in this study. Thus, it was not possible to determine if the amount of particles retained in lungs decreased with increasing recovery time. Red dots in the bottom panel (Fig. 1c, indicated by arrow heads) show areas of inclusions that were matched to the specific hyperspectral reference library created for nano-TiO_2. Bright inclusions in the control samples did not match with the spectra of nano-TiO_2 (Figs. 1a and b). These results demonstrate dose-dependent deposition and sustained retention of nano-TiO_2 over 28 days following the exposure for both the lowest and the highest doses.

Gene expression analysis

In order to understand the biological implications of tissue particle retention in the absence of inflammation, whole lung gene expression profiling was conducted on samples from all the doses and time points. MAANOVA analysis revealed a total of 3452 probes representing 3070 unique genes significantly differentially expressed in response to low, medium and high doses of nano-TiO_2 instillation on post-exposure days 1, 3 and 28. Changes in gene expression were considered significant if they showed p-values of ≤ 0.10 and a fold change ≥ 1.3 in either direction (Supplementary Table 1). Since the present study focused on finding the effects following very low dose exposures that did not show any observable biological response as measured by inflammatory cell counts in BAL fluid, we selected a liberal fold change of ± 1.3 and p-value cut-off of $p \leq 0.1$. These thresholds are aligned with the recommended cut-offs by Shi et al. (2008). These authors suggested the use of fold change ranking in conjugation with a flexible (non-stringent) p-value threshold in order to generate reproducible differentially expressed gene lists (Shi et al., 2008).

A principal component analysis (PCA) on all of the differentially expressed genes revealed a dose and time effect (Supplementary Fig. 1). A total of 1708 genes were significantly differentially expressed on day 1 in at least one of the dose groups compared to controls. Specifically, 462, 691, and 1015 transcripts were affected by nano-TiO_2 treatment in the low, medium, and high dose groups respectively. There were only 60 genes in common across the dose groups (Fig. 2a). Most of the genes on day 1 were up-regulated. A total of 1255 transcripts were differentially expressed relative to controls on day 3 including 693, 652, and 620 in the low, medium, and high dose groups respectively. There were 209 transcripts that were similarly affected across all the dose groups on day 3 (Fig. 2b), and the majority of the genes on day 3 were down-regulated. On day 28, a total of 1198 genes were differentially expressed with 325, 279, and 805 genes changing in the low, medium, and high dose respectively (Fig. 2c), and with a fairly equal number of transcripts being both up- and down-regulated.

Biological functions of differentially expressed genes

GO functional classification was used to identify specific themes in the gene expression patterns following exposure to nano-TiO_2. The

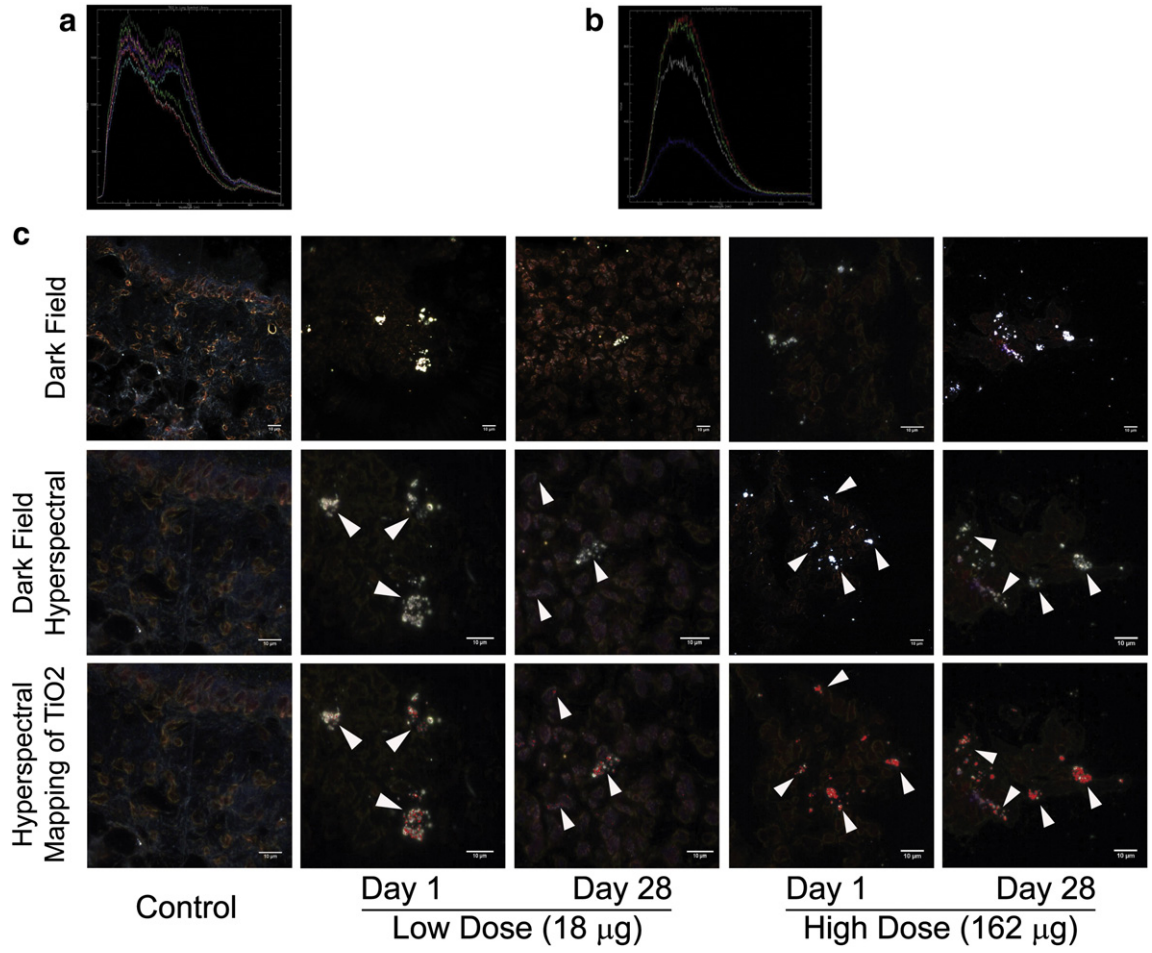

Fig. 1. Identification of nano-TiO_2 particles in lung tissues. Lung tissues from mice harvested 1 and 28 days following a single intratracheal instillation of low (18 μg) and high (162 μg) doses of nano-TiO_2 were subjected to visible and near-infrared (VNIR) hyperspectral imaging to identify particle retention in these tissues. (a) Reference spectral library from nano-TiO_2 exposed tissue. (b) Reference spectral library from control tissue. (c) Dark field images from nano-TiO_2 exposed tissues (upper panel). Dark field hyperspectral images from nano-TiO_2 exposed tissues identifying these nanoparticles, which appeared as aggregates of white inclusions (middle panel). Hyperspectral mapping of nano-TiO_2 in these tissues appeared as red dots or aggregates (bottom panel).

differentially expressed genes were analyzed using DAVID; biological processes with a Fisher's exact p-value ≤ 0.05 (Benjamini–Hochberg corrected) were considered significantly enriched. The common and unique biological processes significantly enriched in different dose groups across the time points are shown in Fig. 3.

Biological processes affected on day 1. The top common biological process altered on day 1 in all three doses consisted of 252 genes (Supplementary Table 2) implicated in immune/inflammatory responses, and was associated with five specific GO terms: immune response [GO:0006955], response to wounding [GO:0009611], inflammatory response [GO:0006954], response to organic substance [GO:0010033], and chemotaxis [GO:0006935] (Fig. 3; day 1, common GO processes). In addition to the immune response, genes in the medium dose group were implicated in various types of metabolism including: fatty acid metabolic process [GO:0006631], and lipid [GO:0006638] and glycerol [GO:0006662] metabolic processes (Fig. 3; day 1, unique GO processes). Genes over-represented in these GO processes were predominantly down-regulated. Unique biological processes affected in the high dose group included: lipid biosynthetic process [GO:0008610], and cholesterol metabolic process [GO:0008203], cell proliferation [GO:0008283], DNA replication [GO:0006260], and extracellular matrix organization [GO:0030198] (Fig. 3; day 1, unique GO processes).

Biological processes affected on day 3. Genes expressed on day 3 were mainly involved in muscle development and/or muscle contraction processes, as indicated by 5 closely related GO biological processes commonly enriched in all 3 dose groups: cytoskeleton organization [GO:0007010], muscle organ development [GO:0007517], actin filament-based process [GO:0030029], muscle contraction [GO:0006936], and striated muscle tissue development [GO:0014706] (Fig. 3; day 3, common GO processes). A complete list of 66 genes that were over-represented on day 3 implicated in muscle development and function is provided in Supplementary Table 3. Unique processes altered in the medium dose group included microtubule-based movement [GO:0007017, GO:0007018]. Uniquely altered processes in the low dose group included homeostatic process [GO:0042592], ion homeostasis [GO:0050801], and regulation of body fluid levels [GO:0050878] (Fig. 3; day 3, unique GO processes).

Biological processes affected on day 28. Muscle regulation (muscle contraction [GO:0006936] and striated muscle tissue development [GO:0060537]) were commonly affected in the low and medium dose groups (Fig. 3; day 28, common GO processes) and consisted of 27 affected genes in these groups (Supplementary Table 4). Some of these processes were also altered on day 3. Inflammatory response (Fig. 3; day 28, unique GO processes) was uniquely altered in the high dose group; calcium ion homeostasis [GO:0055074], homeostatic process

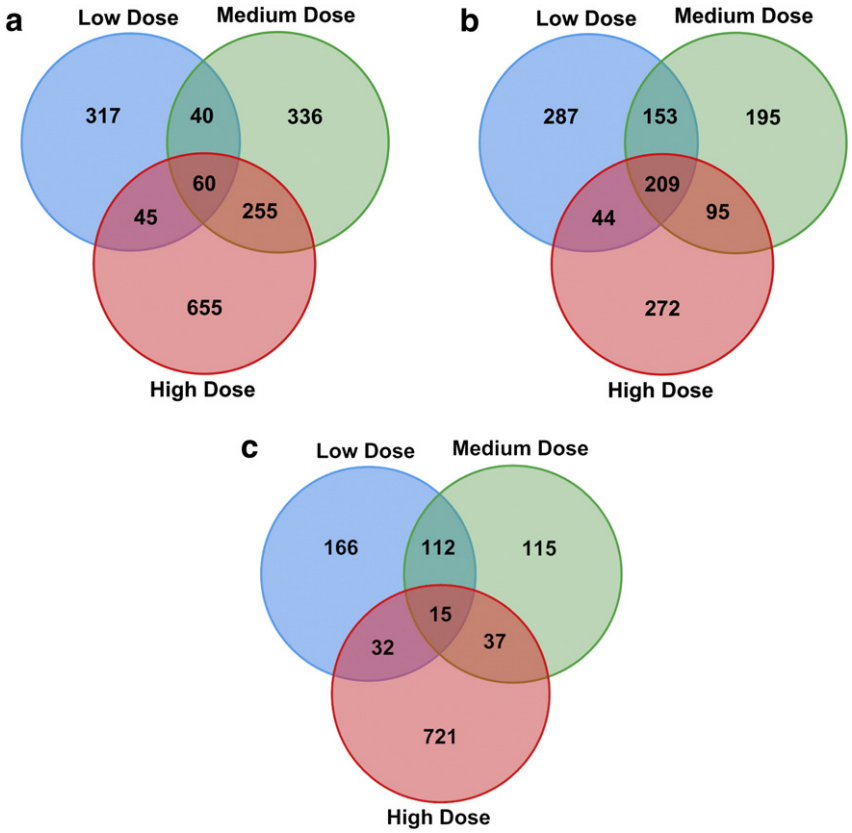

Fig. 2. Venn diagrams showing the overlap of genes that were significantly differentially expressed in response to low (18 μg), medium (54 μg), and high (162 μg) doses of nano-TiO_2 exposure on (a) day 1, (b) day 3, and (c) day 28 post-instillation.

[GO:0042592], and cation homeostasis [GO:0055080] were unique to medium dose group.

Biological pathway analysis

Canonical pathway analysis was conducted using IPA tools. A total of 14 pathways were commonly significantly enriched across all treatment groups (Table 2). There were 7 uniquely affected pathways on 3 days post-exposure, and 4 uniquely perturbed pathways on day 28. Consistent with affected GO processes, the immune-inflammatory response pathway was commonly affected on day 1. Calcium signaling, actin cytoskeleton, and fatty acid metabolism pathways were perturbed on day 3. The hepatic fibrosis/hepatic stellate cell activation pathway was significantly affected on day 28. A total of 56 genes were related to the hepatic fibrosis/hepatic stellate cell activation pathway and these were affected across all dose groups.

qPCR validation of microarray results

A large subset of genes spanning major biological processes/pathways altered by the treatment was selected for qPCR validation. These focused primarily on genes that are associated with inflammation, acute phase response, ion transport, calcium ion binding, and muscle contraction. The qPCR results are presented in Fig. 4 and Supplementary Table 5. Out of the 84 pro-inflammatory genes present on the inflammatory chemokine and cytokine array, 74 genes were differentially expressed (1.3 fold in either direction; $p \leq 0.1$) in at least one dose within at least one time point. Of the 42 genes analyzed by custom array, 38 were significantly altered in treated relative to control mice. A complete list of the 112 validated genes from qPCR experiments is provided in Supplementary Table 5. Sixty-two of the 112 genes were common to both microarray and qPCR (Fig. 4). A correlation analysis performed on the fold changes of 62 validated genes showed high correlation as indicated by the Spearman's rank correlation rho (r) value of 0.89 ($p \leq 0.0001$) (Supplementary Fig. 2).

Tissue expression of pro-inflammatory chemokines and cytokines

Most of the inflammatory modulators are synthesized and stored in an endogenous pool; many of them require activation at the post-transcriptional and translational level. Upon stimulation, these endogenous pools are mobilized therefore the cells/tissues do not immediately require fresh synthesis of mRNA. Therefore, in order to be sure that we did not miss anything in the low dose group by focusing on transcriptional changes we assessed protein levels of 31 chemokines, cytokines, and their receptors. Due to the limited availability of biological material, we used a multiplex ELISA assay and therefore not all selected chemokines and cytokines for protein analysis are matched with those that showed changes in expression at the gene level. Nineteen of the 31 proteins examined were more expressed on day 1 (T helper (Th)-1 and Th-2 cytokines; e.g., IL-1b, IL-2, IL-5, IL-9, IL-10, IL-12, IL-13, IL-17, G-CSF, and GM-CSF) in at least one of the dose groups. Seven proteins were significantly up-regulated on day 3 (CCL3, CCL4, FGF Basic, MCSF, CXCL9, CXCL2, and VEGF) and 8 on day 28 (IL-12(p40), CCL3, CCL4, FGF Basic, MCSF, CXCL9, CXCL2, and VEGF) compared to their matched controls (Fig. 5). None of the up-regulated proteins in the low dose group from day 1 samples showed corresponding increases at the mRNA level. Only four proteins (CCL2, CCL3, CCL4, and CXCL1) showed corresponding increases in mRNA levels in the medium and high dose groups.

Comparison of nano-TiO_2 whole body inhalation and intra-tracheal instillation studies

In a previous study we analyzed pulmonary gene expression profiles of C57BL/6 mice that were subjected to whole body inhalation of

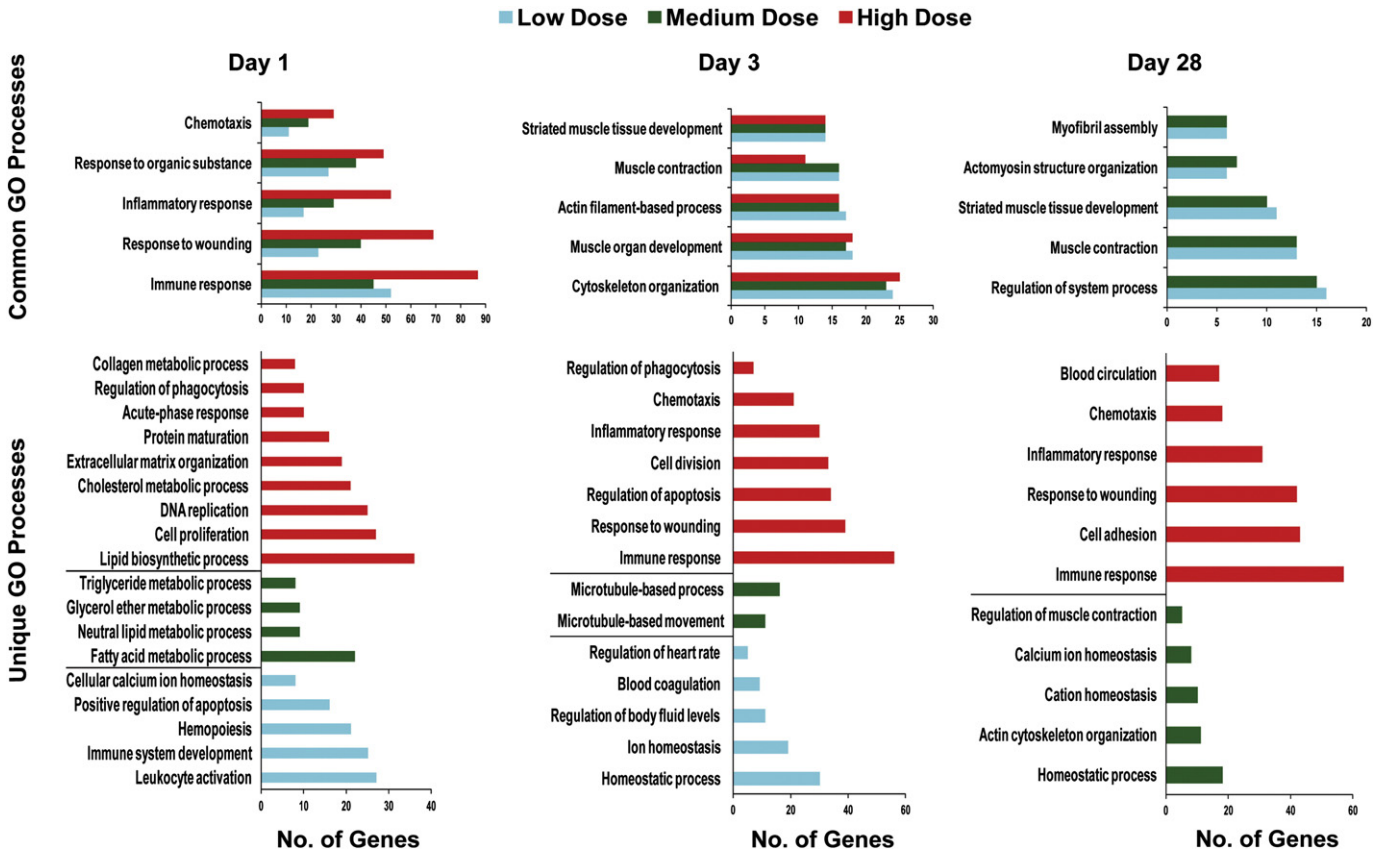

Fig. 3. Gene ontology (GO) analysis of differentially expressed genes. The upper panel shows the GO biological processes that were enriched and were in common among the low, medium, and high dose groups. The lower panel indicates GO biological processes that were uniquely enriched in the low, medium, and high dose groups. Columns from left to right present the enrichment of GO biological processes on days 1, 3, and 28, respectively. Results from low, medium, and high dose groups are shown in blue, green, and red bars respectively.

42 mg/m^3 of nano-TiO_2 1 h/day for 11 consecutive days (Halappanavar et al., 2011; Hougaard et al., 2010). Global gene expression was assessed 5 days following the last exposure. The phenotype was characterized by neutrophilic inflammation as measured by BAL cellular differential counts. A parallel analysis of pulmonary gene expression profiles showed differential expression of 355 genes with a fold change of at least ± 1.3 ($p \leq 0.1$). These genes mainly belonged to immune-inflammatory response, acute phase response, chemotaxis, and complement activation processes. In the present study, similar neutrophil-dominant inflammation was observed following intratracheal instillation. Moreover, approximately 57% (201/355, $p \leq 0.1$ and fold change ± 1.3; Supplementary Table 6) of those genes were commonly differentially regulated in the lungs in one or more of the treatment conditions. In addition to taking part in immune-inflammatory responses, these common genes also play a role in muscle contraction, ion/calcium ion homeostasis, and fatty acid/lipid metabolic processes. For example, some of these commonly affected genes include *Il1b*, *Saa3*, *cxcl5*, *Ly6f*, *Slc26a4*, *Lcn2*, *Noxo1*, *cxcl12*, *ccl7*, *ccl9*, *ccl2*, *ccl17*, *ccl12*, *Atp1a2*, *Myom2*, *Tnnt2*, *Fasn*, *Aacs*, and *Ch25h*.

Discussion

In this study lung gene expression profiles of mice exposed to 3 different doses of nano-TiO_2 were analyzed at three different post-exposure time points in parallel with the analysis of particle retention in the lungs.

Enhanced darkfield imaging of lung tissue sections demonstrated that intratracheal instillation of nano-TiO_2 resulted in non-uniform deposition of particles (seen as white inclusions; Fig. 1c) throughout the lung regions at all of the examined doses and post-exposure time points. Near-infrared hyperspectral image analysis confirmed that the highly illuminated white inclusions observed in treated samples corresponded specifically to nano-TiO_2 (shown in red; Fig. 1c). Particle retention was observed more in the high dose group than the low doses. Interestingly, mice exposed to the low dose did not exhibit any signs of pulmonary neutrophilic inflammation, but noticeable particle retention was observed. Moreover, particles were also observed in the lungs of mice exposed to the high dose group at 28 days post-exposure when inflammation is primarily resolving. These findings suggest: (1) the low dose (18 μg) was not sufficient to induce neutrophil influx in BAL, or (2) acute inflammation as measured by increased number of inflammatory cells in BAL induced immediately after a low dose of particles was resolved within 24 h.

Relatively few studies have shown the retention of NPs in the lung. Hougaard et al. (2010) found that 21% of the deposited pulmonary dose in mice exposed by inhalation to the same nano-TiO_2 for 11 consecutive days at 42 mg/m^3 for 1 h was retained 26 days after terminating the exposure. Each day of this dosing regimen corresponds to a single 4-hour daily exposure at the current Danish occupational exposure limit of 9.75 mg/m^3 TiO_2. It is suggested that phagocytic uptake and/or phagocyte-mediated translocation are the key clearance mechanisms for particles deposited in airways and alveoli. However, various studies have found that nano-scale particles evade these mechanisms and penetrate interstitial regions of lungs. For example, Geiser et al. (2008) demonstrated that 20 nm TiO_2-NPs are not recognized and cleared by phagocytes in rat lungs within the first 24 h following exposure. Instead, NPs are engulfed within the first 24 h via non-specific processes occurring during the phagocytosis of the surrounding material (Geiser et al., 2008). These findings suggest that most of the TiO_2-NPs escape the immediate and primary clearance mechanisms, and are thus free to

Table 2
Significantly enriched biological pathways in the low, medium and high doses of nano-TiO_2 exposed mice sampled 1, 3 or 28 days following the single initial exposure.

Pathways	Low dose		Medium dose		High dose	
	No. of genes	Fisher's *p*-value	No. of genes	Fisher's *p*-value	No. of genes	Fisher's *p*-value
Day 1						
Acute phase response signaling	8	0.040	21	0.000	44	0.000
LXR/RXR activation	7	0.019	21	0.000	40	0.000
Atherosclerosis signaling	8	0.005	10	0.015	27	0.000
LPS/IL-1 mediated inhibition of RXR function	9	0.047	15	0.015	26	0.000
Hepatic fibrosis/hepatic stellate cell activation	9	0.005	16	0.000	24	0.000
Communication between innate and adaptive immune cells	10	0.000	8	0.004	14	0.000
Role of pattern recognition receptors in recognition of bacteria and viruses	10	0.000	8	0.037	13	0.005
IL-17A signaling in fibroblasts	4	0.009	4	0.049	12	0.000
Crosstalk between dendritic cells and natural killer cells	5	0.029	7	0.028	10	0.013
TNFR2 signaling	5	0.000	4	0.026	7	0.001
MIF regulation of innate immunity	7	0.000	5	0.021	6	0.032
MIF-mediated glucocorticoid regulation	6	0.000	4	0.037	5	0.041
Role of IL-17A in psoriasis	2	0.023	3	0.007	5	0.000
Pathogenesis of multiple sclerosis	2	0.014	2	0.040	4	0.001
Day 3						
Calcium signaling	22	0.000	23	0.000	17	0.000
ILK signaling	16	0.000	17	0.000	12	0.026
Actin cytoskeleton signaling	14	0.006	17	0.001	13	0.044
Cellular effects of sildenafil	11	0.002	14	0.000	9	0.044
Fatty acid metabolism	11	0.001	8	0.025	8	0.044
Hepatic fibrosis/hepatic stellate cell activation	9	0.026	12	0.002	13	0.001
Aryl hydrocarbon receptor signaling	9	0.022	12	0.001	12	0.003
Day 28						
Hepatic fibrosis/hepatic stellate cell activation	13	0.000	12	0.000	12	0.013
Signaling by Rho family GTPases	9	0.020	7	0.047	17	0.017
Cdc42 signaling	6	0.025	5	0.036	11	0.019
Differential regulation of cytokine production in intestinal epithelial cells by IL-17A and IL-17F	2	0.050	2	0.035	4	0.010

translocate to interstitial regions. Zhu et al. (2008) compared 22 nm and 280 nm iron oxide particles and found that 22 nm particles were more readily embedded in the lung interstitium (Zhu et al., 2008). Size-dependent particle uptake by macrophages was also demonstrated in rats using iridium and polystyrene particles (Semmler-Behnke et al., 2007). Despite the fact that ~50% of inhaled particles were immediately available for uptake by phagocytes in BAL, this study revealed that less than 20% of them were associated with phagocytic macrophages. Hougaard et al. (2010) showed that ~25% of the deposited pulmonary dose is retained up to 5 days, and 21% up to 26 days post-exposure following nano-TiO_2 inhalation in mice. These results collectively suggest that the observed pulmonary particle retention in our present study in all dose groups across the different post-exposure time points could be the combined result of three potential factors: (1) inability to generate sufficient chemotactic signaling to induce phagocytic infiltration; (2) failed phagocytic recognition; and (3) timely engulfment and rapid translocation to interstitial lung spaces and inefficient clearance.

Inflammation is routinely used as a measure of pulmonary response to particle exposures. We thus sought to examine whether the lack of inflammation (low dose) or diminished inflammation (late time point) observed in our study is truly reflective of a lack of biological or toxicological response in the lungs following nano-TiO_2 exposure. To do this, we quantified changes in global pulmonary gene expression for all doses and post-exposure time points in our experiment. As expected, we observed large changes in the expression of genes associated with inflammatory processes, which were both dose- and time-dependent. GO ontology analysis of differentially expressed genes revealed enrichment in four main functional groups; inflammation and immune response, lipid metabolism, muscle regulation, and ion homeostasis. Several genes encoding complements, cytokines, chemokines, and acute phase responders, including *C3*, *Il1b*, *Ccl4*, *Ccl17*, *Cxcl5*, *Saa1*, *Saa2*, *Saa3*, *S100a8*, *S100A9*, and *Nfkbia* were significantly up-regulated in this study, indicating the recruitment of leukocytes, predominantly neutrophils (Saber et al., 2012) and induction of acute phase signaling. Pathway specific PCR arrays containing 84 different cytokines and chemokines were used to confirm the majority of these changes (Fig. 4 and Supplementary Table 6). Although the low dose group did not show any evidence of cellular infiltration in BAL (Saber et al., 2012), various genes associated with inflammation were perturbed in these samples, albeit to a lesser extent than the higher doses. This finding is consistent with the hypothesis that inflammatory signaling occurs even at low doses, but is insufficient to cause measurable influx of inflammatory cells in lung lavages.

Despite the lack of neutrophilic infiltration in BAL and the somewhat subtle changes in the expression of inflammatory genes in lung tissues of mice in the low dose group, we observed significant increases in protein synthesis of 17 inflammatory mediators in these samples including IL-2, IL-5, IL-9, IL-10, IL-12, IL-13, IL-17, CCL11, GM-CSF, IFN-g, CXCL1, CCL2, CCL3, CCL4, FGF-basic, MCSF, and VEGF. These results again suggest that exposure to the low dose led to the initiation of transient chemotactic signaling, but that this signaling may have been below the threshold level required to initiate a respiratory burst leading to neutrophil influx in BAL. Alternately, the rapid interstitialization of particles may have resulted in activation of interstitial macrophages, creating a chemotactic gradient in lungs that shifts the inflammatory influx to the interstitium leading to decreased cellular influx in the alveolar space (Ferin et al., 1992; Oberdorster et al., 1992).

Differential cellular count of inflammatory cells in BAL fluid is an accepted marker of lung response following exposure to particles (Warheit et al., 1991). Based on lack of inflammatory cell influx in BAL fluid, many studies have claimed that TiO_2 particles are not toxic. Our results show no increases in inflammatory cell influx in BAL fluid following exposure to low doses of TiO_2. However, our microarray results revealed significant alteration in the expression of a few inflammatory genes. ELISA

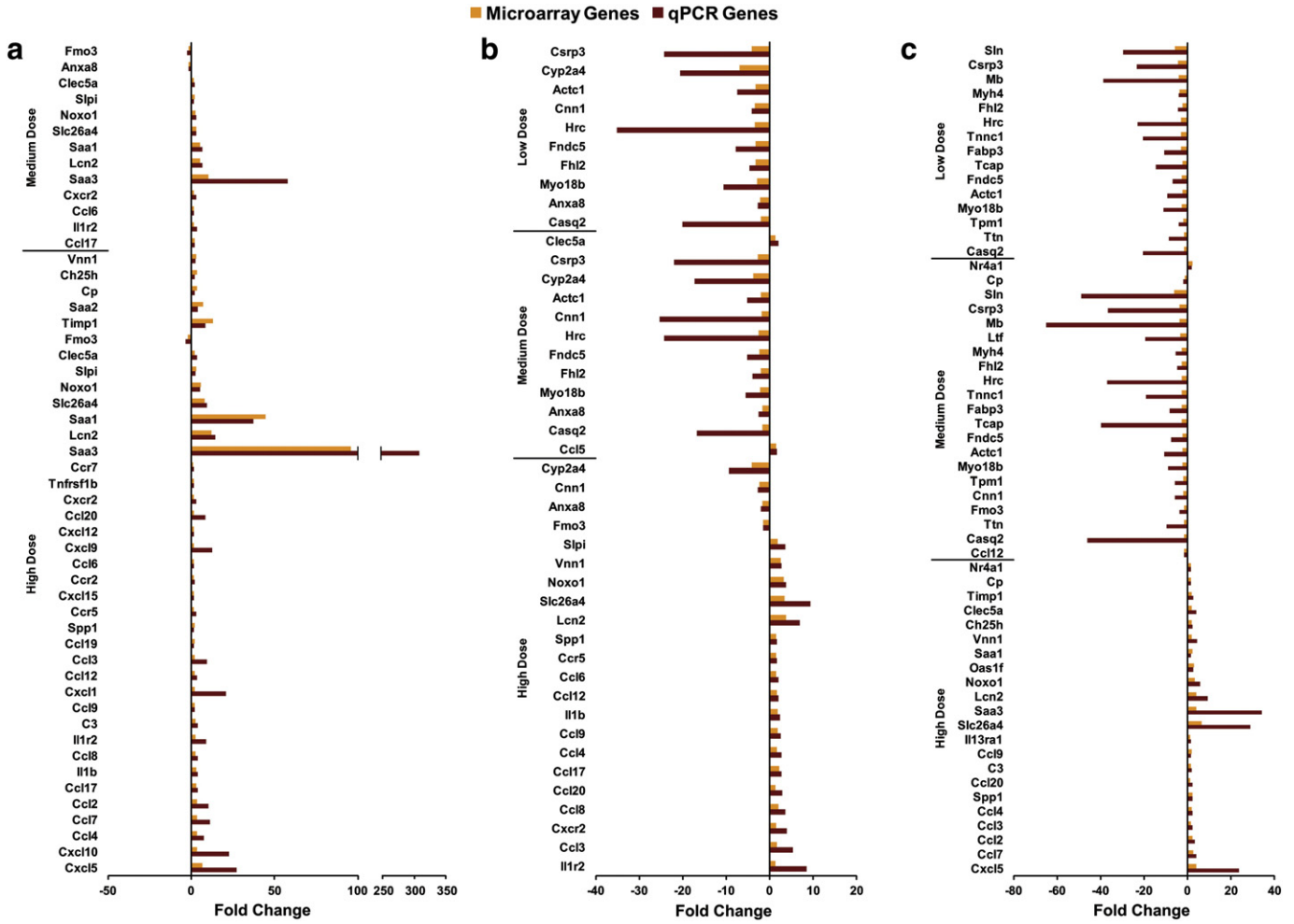

Fig. 4. Validation of genes identified as significantly differentially expressed in microarray experiment by qPCR. A total of 62 genes from the microarray experiment were also examined in the qPCR experiment in either of the low, medium or high dose groups in samples from: (a) day 1, (b) day 3, and (c) day 28 post-instillation periods. All genes from microarray and qPCR experiments had the same directional fold changes of at least ± 1.3 with a *p*-value of ≤0.1. Please note that no genes from the low dose group on day 1 met this threshold. The bars in yellow represent transcripts measured in microarray experiments and the bars in brown represent transcripts measured with qPCR.

assays revealed upregulated protein synthesis of several inflammatory modulators including CXCL1 and CXCL2. These results suggest that differential BAL counts are not sensitive enough to pick up effects following low dose exposures, and that assessment of genes and proteins associated with inflammation may provide a more sensitive measure of the pulmonary response.

Importantly, many of the genes in the perturbed pathways noted in this study were also up-regulated in mouse lungs following whole-body inhalation (1 h/day for 11 consecutive days) of 40 mg UV-Titan/m^3 of the same nano-TiO_2 particles tested by Halappanavar et al. (2011). The 40 mg TiO_2/m^3/h exposure corresponds to the 8-hr time weighted average (TWA) Danish occupational exposure limit (At-vejledning, 2007). If it is assumed that 9% of the inhaled particle mass ends up in the respiratory system, then the total volume of inhaled air per hour would be 1.8 l/h (Hougaard et al., 2010) in an 8 h working day. In comparison, the doses 18, 54 and 162 μg/mouse used in the present study are the equivalent of 1.5, 5 and 15 working days at the Danish occupational exposure level for TiO_2 (6.0 mg Ti/m^3–9.75 mg TiO_2/m^3), respectively. Thus, the inhalation dose is similar to the 54 μg dose used in the present study and indicates that the responses observed are similar to those observed following exposure to the 54 μg dose on day 1. These results demonstrate that the inflammatory responses following bolus administration of nano-TiO_2 are comparable to those observed following inhalation, a physiological route of exposure to particles in the environment. Thus, it is reasonable to argue that the low-dose instillation results observed in this study are relevant to those from inhalation study by Halappanavar et al. (2011).

Chronic persistent inflammation, pulmonary fibrosis, and lung tumors have been documented in rats following chronic and subchronic inhalation of low toxicity ultrafine titanium dioxide particles (reviewed in (Johnston et al., 2009)). However, it has been argued that these studies use very high doses that lead to excessive accumulation of particles and saturation of phagocyte-mediated clearance mechanisms in lungs, and are thus less physiologically relevant. Although very little is known about the effects of prolonged retention of low levels of particles in the lungs, retention and accumulation of particles over extended periods of time are postulated to lead to increased lung particle burden and enhanced risk of developing small airway cancer. In the present study we extend our dose down to much lower than what has been used in earlier studies (Ferin et al., 1992; Grassian et al., 2007; Renwick et al., 2004; Warheit et al., 2007) and reviewed in Johnston et al. (2009) and demonstrate significant retention of particles in the lungs even at this low dose. We hypothesize that low levels of particle retention and accumulation over time (leading to persistent particle presence in alveolar or interstitial spaces) might hinder air movement, alter lung smooth muscle contraction activities, and induce tissue foreign body reaction leading to tissue scaring and tissue fibrosis. In support of this hypothesis gene expression and pathway analysis revealed muscle regulation and ion homeostasis to be significantly altered in the nano-TiO_2 exposed mouse lungs. Specifically, we observed down-regulation of several genes

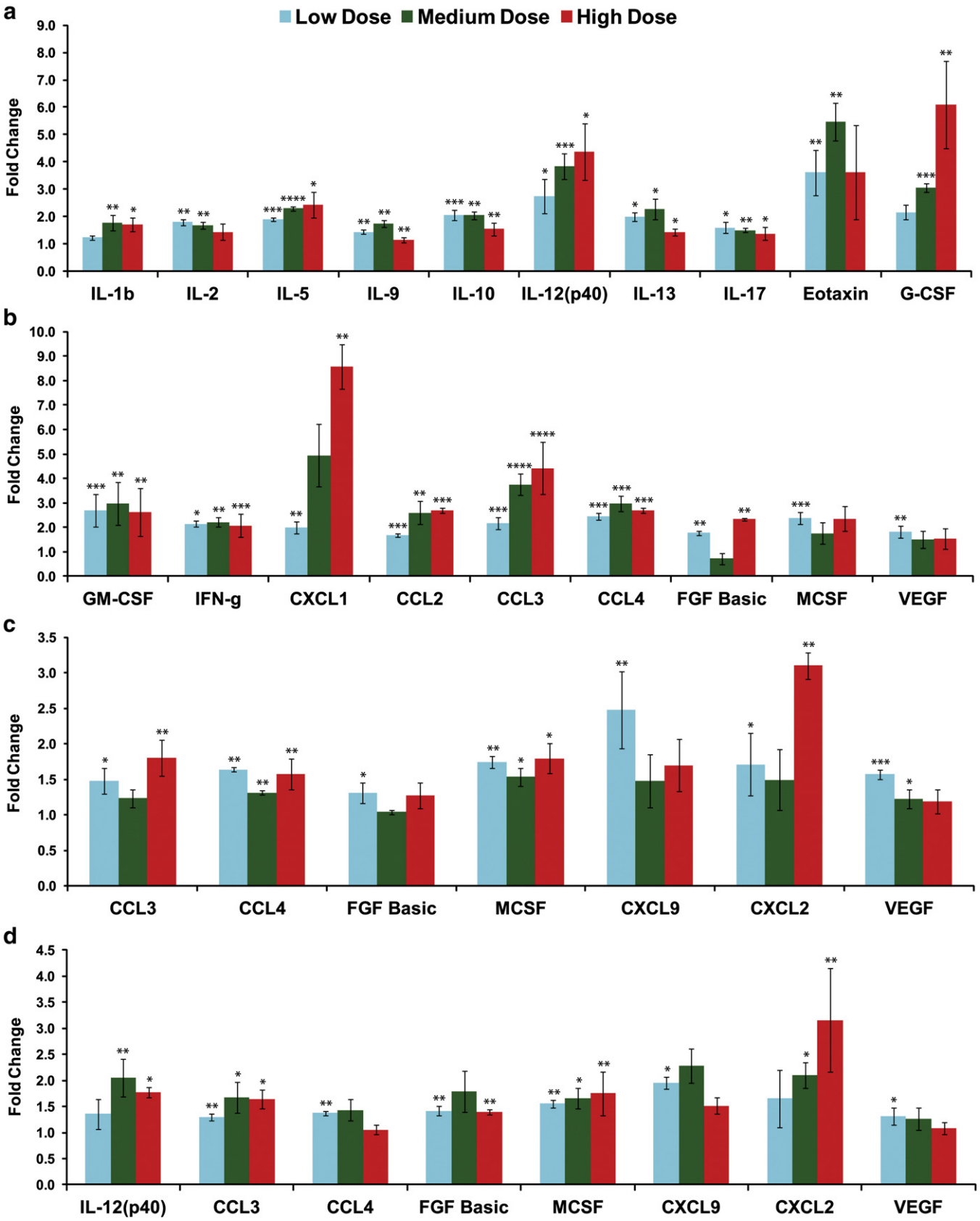

Fig. 5. Analysis of proteins involved in pro-inflammatory response in the lungs of experimental mice exposed to nano-TiO_2 compared to controls on (a) and (b) day 1, (c) day 3, and (d) day 28 post-instillation periods. The bars in blue, green, and red represent proteins expressed in response to low (18 μg), medium (54 μg), and high (162 μg) doses of nano-TiO_2 exposure respectively. The y-axis shows the fold change ± SE of exposed relative to control mice. Statistical significance was calculated using Student's *t*-test. $^{*}p \leq 0.1$; $^{**}p \leq 0.05$; $^{***}p \leq 0.01$; and $^{****}p \leq 0.001$.

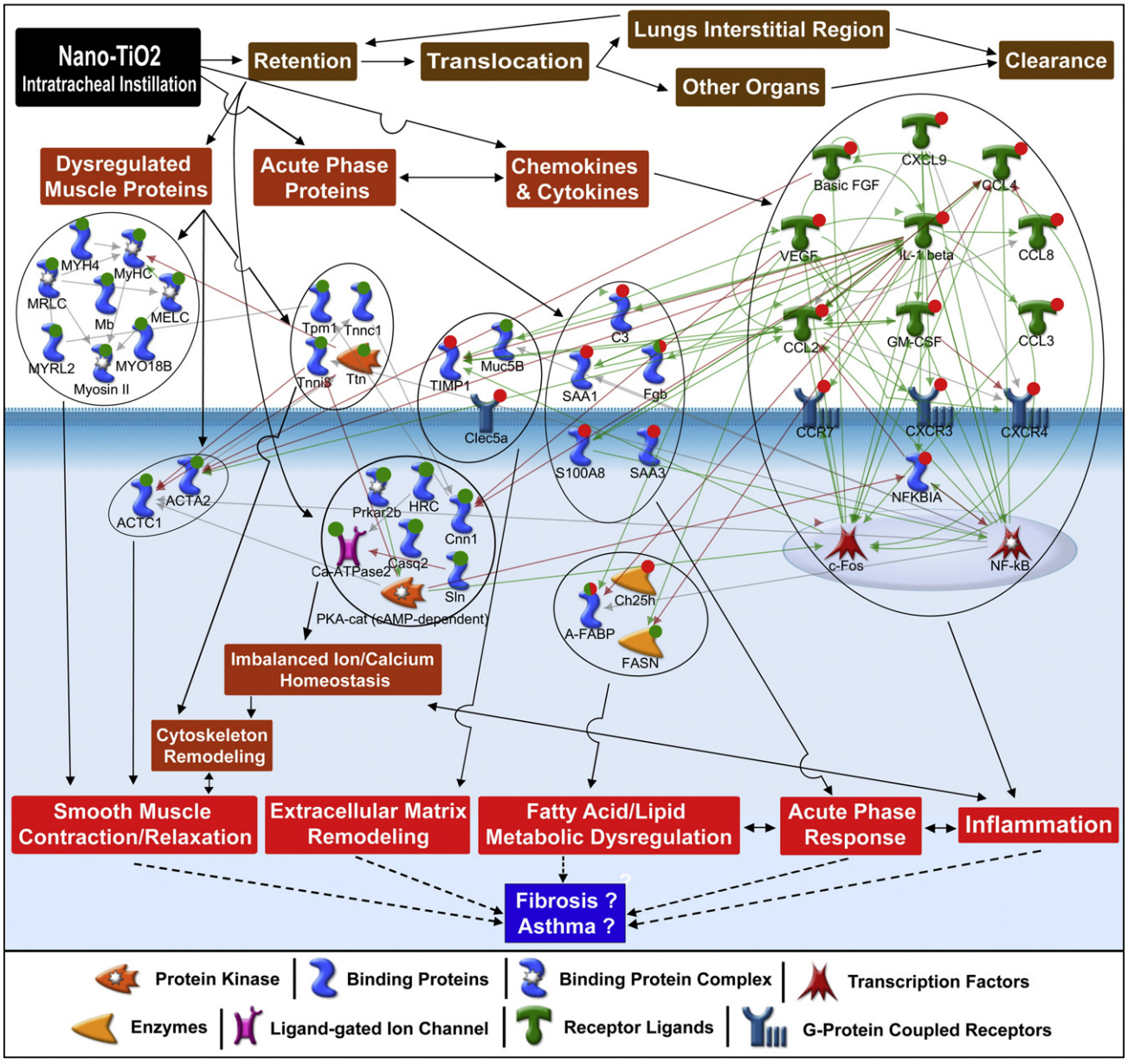

Fig. 6. The associations and pathways that are perturbed following low-dose exposure to nano-TiO_2 that link particle retention and response to potential longer-term health outcomes. Genes that are shown with a red or green circle were up- or down-regulated, respectively. Genes with circles that are colored both red and green circles had mixed expression (up-regulated at one time point and down-regulated in another time point). NF-κB, c-Fos and cyclic AMP dependent PKA are indirectly connected to the genes shown; however, are not specifically altered in our data set. The green arrows connecting genes/proteins represent positive regulation/activation; the brown arrows connecting genes/proteins represent negative regulation/inhibition; the grey arrows connecting genes/proteins represent unspecified regulation.

(*Tnni3*, *Tnnt2*, *Tpm1*, *Myh4*, *Myh6*, *Actc1*, *S100a8*, and *Actn2*) that regulate muscle contraction and calcium homeostasis 3 and 28 days post-instillation. The response was much more pronounced on day 28, with dramatic down-regulation of several genes implicated in ion homeostasis, calcium binding, muscle contraction and development, and cytoskeleton organization (Fig. 4). Of note, the perturbations in the expression of genes associated with ion homeostasis and muscle functions were independent of the inflammatory status. The effects on ion homeostasis were prominent only on days 3 and 28 following low and medium dose exposures; in contrast, these time points and doses showed little or no inflammation. Similar resolution of inflammation in the presence of substantial particle burden was also reported in a study conducted by Ferin et al. (1992). These authors suggested that inflammatory reaction could be an indication of lung responses occurring during the exposure process and does not necessarily reflect the lung burden of particles. Our results together with those of Ferin et al. (1992) suggest that inflammation may not be the underlying factor influencing the gene expression changes associated with ion homeostasis; rather, these effects are potentially the results of persistent and prolonged retention of particles in the lungs. Thus, we speculate that the absence of inflammation resulting in the prolonged confinement of particles to one place is a prerequisite to sequestration of ions around the particle deposition sites, leading to imbalances in ion homeostasis and deregulation of muscle functions. Although a clear evidence in support of this hypothesis could not be provided in the present study, our results are indicative of particle-specific effects.

Calcium influx and signaling regulate neutrophil activation and neutrophil mediated inflammatory processes in the lungs (Burgos et al., 2011; Tintinger et al., 2005). Imbalance in calcium homeostasis following

pulmonary inflammation severely affects contraction of airway smooth muscle in the lungs (Perez-Zoghbi et al., 2009). Gatti et al. (2008) used a rodent implantation model to evaluate the effects of different nanomaterials and corresponding bulk materials implanted for 6–12 months on subcutaneous or muscular tissues and found that sites implanted with TiO_2-NPs developed intramuscular foreign body granulomas and moderate fibrosis surrounded by macrophages and giant cells (Gatti et al., 2008). Moreover, nano-TiO_2 exposure caused an increase in the generation of Fe, Na, S, and P ions close to the particle deposition site and spherical Ca–P precipitates containing Fe and Zn, specifically observed at 12 months post-implantation period. Sequestration of ions, such as Ca and P, renders them biologically unavailable (Gatti et al., 2008). Since these ions play an important role in many signal transduction pathways, their precipitation will lead to altered homeostasis and imbalance in cellular functioning. Although we could not confirm the formation of granulomas or analyze ion sequestration at the site of particle deposition, substantive alterations in the expression of several genes involved in ion homeostasis and muscle contraction suggest that prolonged accumulation of particles could trigger airway smooth muscle pathology, and increase the risk of developing lung conditions such as asthma, chronic obstructive pulmonary disease, and pulmonary fibrosis (Byrne and Baugh, 2008).

In conclusion (Fig. 6), our combined data indicate that a significant amount of nano-TiO_2 particles is deposited in the lungs even following exposure to very low doses, and that particles are retained in the lungs for at least 28 days. Although further experiments are needed to confirm the ideas presented in the present study, our results imply that particle accumulation over an extended timeframe together with alterations in the expression of several genes associated with ion homeostasis and muscle function may potentially interfere with calcium, ion, and lipid homeostasis, and affect pulmonary smooth muscle contraction. Prolonged disturbances in ion homeostasis and airway smooth muscle functioning can potentially contribute to the development of lung diseases such as pulmonary fibrosis, asthma, and even lung cancers. Moreover, statistically significant changes in the expression of several genes and proteins involved in vital lung functions in the absence of any observable inflammation call for a careful re-evaluation of particle induced lung toxicity.

Funding

This work was supported by the Health Canada's Genomics Research and Development Initiative, Chemicals Management Plan 2-Nano, and Internal A-base Research Funds, as well as the Danish NanoSafety Centre co-funded by the Danish Work Research Foundation.

Conflicts of interest

The authors declare that there are no conflicts of interest.

Appendix A. Supplementary data

Supplementary data to this article can be found online at http://dx.doi.org/10.1016/j.taap.2013.03.018.

References

At-vejledning, 2007. Grænseværdier for stoffer og materialer. At-vejledning C.0.1. København. Arbejdstilsynet 1–84.
Benjamini, Y., Hochberg, Y., 1995. Controlling the false discovery rate: a practical and powerful approach to multiple testing. J. R. Stat. Soc. Ser. B Methodol. 57, 289–300.
Bermudez, E., Mangum, J.B., Asgharian, B., Wong, B.A., Reverdy, E.E., Janszen, D.B., Hext, P.M., Warheit, D.B., Everitt, J.I., 2002. Long-term pulmonary responses of three laboratory rodent species to subchronic inhalation of pigmentary titanium dioxide particles. Toxicol. Sci. 70, 86–97.
Bermudez, E., Mangum, J.B., Wong, B.A., Asgharian, B., Hext, P.M., Warheit, D.B., Everitt, J.I., 2004. Pulmonary responses of mice, rats, and hamsters to subchronic inhalation of ultrafine titanium dioxide particles. Toxicol. Sci. 77, 347–357.
Burgos, R.A., Conejeros, I., Hidalgo, M.A., Werling, D., Hermosilla, C., 2011. Calcium influx, a new potential therapeutic target in the control of neutrophil-dependent inflammatory diseases in bovines. Vet. Immunol. Immunopathol. 143, 1–10.
Byrne, J.D., Baugh, J.A., 2008. The significance of nanoparticles in particle-induced pulmonary fibrosis. Mcgill J. Med. 11, 43–50.
Cleveland, W.S., 1979. Robust locally weighted regression and smoothing scatterplots. J. Am. Stat. Assoc. 74, 829–836.
Cui, X., Qiu, J.T.H.J., Blades, N.J., Churchill, G.A., 2005. Improved statistical tests for differential gene expression by shrinking variance components estimates. Biostatistics 6, 59–75.
Ferin, J., Oberdorster, G., Penney, D.P., 1992. Pulmonary retention of ultrafine and fine particles in rats. Am. J. Respir. Cell Mol. Biol. 6, 535–542.
Gatti, A.M., Kirkpatrick, J., Gambarelli, A., Capitani, F., Hansen, T., Eloy, R., Clermont, G., 2008. ESEM evaluations of muscle/nanoparticles interface in a rat model. J. Mater. Sci. Mater. Med. 19, 1515–1522.
Geiser, M., Casaulta, M., Kupferschmid, B., Schulz, H., Semmler-Behnke, M., Kreyling, W., 2008. The role of macrophages in the clearance of inhaled ultrafine titanium dioxide particles. Am. J. Respir. Cell Mol. Biol. 38, 371–376.
Grassian, V.H., O'Shaughnessy, P.T., Adamcakova-Dodd, A., Pettibone, J.M., Thorne, P.S., 2007. Inhalation exposure study of titanium dioxide nanoparticles with a primary particle size of 2 to 5 nm. Environ. Health Perspect. 115, 397–402.
Halappanavar, S., Jackson, P., Williams, A., Jensen, K.A., Hougaard, K.S., Vogel, U., Yauk, C.L., Wallin, H., 2011. Pulmonary response to surface-coated nanotitanium dioxide particles includes induction of acute phase response genes, inflammatory cascades, and changes in microRNAs: a toxicogenomic study. Environ. Mol. Mutagen. 52, 425–439.
Heinrich, U., Fuhst, R., Rittinghausen, S., Creutzenberg, O., Bellmann, B., Koch, W., Levsen, K., 1995. Chronic inhalation exposure of Wistar rats and two different strains of mice to diesel engine exhaust, carbon black, and titanium dioxide. Inhal. Toxicol. 7, 533–556.
Hougaard, K.S., Jackson, P., Jensen, K.A., Sloth, J.J., Loschner, K., Larsen, E.H., Birkedal, R.K., Vibenholt, A., Boisen, A.M., Wallin, H., Vogel, U., 2010. Effects of prenatal exposure to surface-coated nanosized titanium dioxide (UV-Titan). A study in mice. Part. Fibre Toxicol. 7, 16.
Huang da, W., Sherman, B.T., Lempicki, R.A., 2009. Systematic and integrative analysis of large gene lists using DAVID bioinformatics resources. Nat. Protoc. 4, 44–57.
IARC, 2010. IARC monographs on the evaluation of carcinogenic risks to humans: carbon black, titanium dioxide, and talc. IARC Monogr. Eval. Carcinog. Risks Hum. 93, 1–413.
Iavicoli, I., Leso, V., Fontana, L., Bergamaschi, A., 2011. Toxicological effects of titanium dioxide nanoparticles: a review of in vitro mammalian studies. Eur. Rev. Med. Pharmacol. Sci. 15, 481–508.
Johnston, H.J., Hutchison, G.R., Christensen, F.M., Peters, S., Hankin, S., Stone, V., 2009. Identification of the mechanisms that drive the toxicity of $TiO_{(2)}$particulates: the contribution of physicochemical characteristics. Part. Fibre Toxicol. 6, 33.
Katsnelson, B., Privalova, L.I., Kuzmin, S.V., Degtyareva, T.D., Sutunkova, M.P., Yeremenko, O.S., Minigalieva, I.A., Kireyeva, E.P., Khodos, M.Y., Kozitsina, A.N., Malakhova, N.A., Glazyrina, J.A., Shur, V.Y., Shishkin, E.I., Nikolaeva, E.V., 2010. Some peculiarities of pulmonary clearance mechanisms in rats after intratracheal instillation of magnetite (Fe_3O_4) suspensions with different particle sizes in the nanometer and micrometer ranges: are we defenseless against nanoparticles? Int. J. Occup. Environ. Health 16, 508–524.
Kerr, M.K., 2003. Design considerations for efficient and effective microarray studies. Biometrics 59, 822–828.
Kerr, M.K., Churchill, G.A., 2007. Statistical design and the analysis of gene expression microarray data. Genet. Res. 89, 509–514.
Khatri, P., Sirota, M., Butte, A.J., 2012. Ten years of pathway analysis: current approaches and outstanding challenges. PLoS Comput. Biol. 8, e1002375.
Liao, C.M., Chiang, Y.H., Chio, C.P., 2008. Model-based assessment for human inhalation exposure risk to airborne nano/fine titanium dioxide particles. Sci. Total Environ. 407, 165–177.
Liu, R., Yin, L., Pu, Y., Liang, G., Zhang, J., Su, Y., Xiao, Z., Ye, B., 2009. Pulmonary toxicity induced by three forms of titanium dioxide nanoparticles via intra-tracheal instillation in rats. Prog. Nat. Sci. 19, 573–579.
Madl, A.K., Pinkerton, K.E., 2009. Health effects of inhaled engineered and incidental nanoparticles. Crit. Rev. Toxicol. 39, 629–658.
Nemmar, A., Melghit, K., Al-Salam, S., Zia, S., Dhanasekaran, S., Attoub, S., Al-Amri, I., Ali, B.H., 2011. Acute respiratory and systemic toxicity of pulmonary exposure to rutile Fe-doped $TiO_{(2)}$ nanorods. Toxicology 279, 167–175.
Oberdorster, G., Ferin, J., Gelein, R., Soderholm, S.C., Finkelstein, J., 1992. Role of the alveolar macrophage in lung injury: studies with ultrafine particles. Environ. Health Perspect. 97, 193–199.
Oberdorster, G., Finkelstein, J.N., Johnston, C., Gelein, R., Cox, C., Baggs, R., Elder, A.C., 2000. Acute pulmonary effects of ultrafine particles in rats and mice. Res. Rep. Health Eff. Inst. 5–74 (disc 75–86).
Park, E.J., Yoon, J., Choi, K., Yi, J., Park, K., 2009. Induction of chronic inflammation in mice treated with titanium dioxide nanoparticles by intratracheal instillation. Toxicology 260, 37–46.
Perez-Zoghbi, J.F., Karner, C., Ito, S., Shepherd, M., Alrashdan, Y., Sanderson, M.J., 2009. Ion channel regulation of intracellular calcium and airway smooth muscle function. Pulm. Pharmacol. Ther. 22, 388–397.
Renwick, L.C., Brown, D., Clouter, A., Donaldson, K., 2004. Increased inflammation and altered macrophage chemotactic responses caused by two ultrafine particle types. Occup. Environ. Med. 61, 442–447.
Saber, A.T., Jacobsen, N.R., Mortensen, A., Szarek, J., Jackson, P., Madsen, A.M., Jensen, K.A., Koponen, I.K., Brunborg, G., Gutzkow, K.B., Vogel, U., Wallin, H., 2012. Nanotitanium

dioxide toxicity in mouse lung is reduced in sanding dust from paint. Part. Fibre Toxicol. 9, 4.
Semmler-Behnke, M., Takenaka, S., Fertsch, S., Wenk, A., Seitz, J., Mayer, P., Oberdorster, G., Kreyling, W.G., 2007. Efficient elimination of inhaled nanoparticles from the alveolar region: evidence for interstitial uptake and subsequent reentrainment onto airways epithelium. Environ. Health Perspect. 115, 728–733.
Shapiro, S.S., Wilk, M.B., 1965. An analysis of variance test for normality (complete samples). Biometrika 52, 591–611.
Shi, L., Jones, W.D., Jensen, R.V., Harris, S.C., Perkins, R.G., Goodsaid, F.M., Guo, L., Croner, L.J., Boysen, C., Fang, H., Qian, F., Amur, S., Bao, W., Barbacioru, C.C., Bertholet, V., Cao, X.M., Chu, T.M., Collins, P.J., Fan, X.H., Frueh, F.W., Fuscoe, J.C., Guo, X., Han, J., Herman, D., Hong, H., Kawasaki, E.S., Li, Q.Z., Luo, Y., Ma, Y., Mei, N., Peterson, R.L., Puri, R.K., Shippy, R., Su, Z., Sun, Y.A., Sun, H., Thorn, B., Turpaz, Y., Wang, C., Wang, S.J., Warrington, J.A., Willey, J.C., Wu, J., Xie, Q., Zhang, L., Zhang, L., Zhong, S., Wolfinger, R.D., Tong, W., 2008. The balance of reproducibility, sensitivity, and specificity of lists of differentially expressed genes in microarray studies. BMC Bioinformatics 9 (Suppl. 9), S10.
Spearman, C., 1904. The proof and measurement of association between two things. Am. J. Psychol. 15, 72–101.
Tintinger, G., Steel, H.C., Anderson, R., 2005. Taming the neutrophil: calcium clearance and influx mechanisms as novel targets for pharmacological control. Clin. Exp. Immunol. 141, 191–200.
Warheit, D.B., Carakostas, M.C., Hartsky, M.A., Hansen, J.F., 1991. Development of a short-term inhalation bioassay to assess pulmonary toxicity of inhaled particles: comparisons of pulmonary responses to carbonyl iron and silica. Toxicol. Appl. Pharmacol. 107, 350–368.
Warheit, D.B., Webb, T.R., Reed, K.L., Frerichs, S., Sayes, C.M., 2007. Pulmonary toxicity study in rats with three forms of ultrafine-TiO_2 particles: differential responses related to surface properties. Toxicology 230, 90–104.
Wu, H., Kerr, K.M., Cui, X., Churchill, G.A., 2003. MAANOVA: a software package for the analysis of spotted cDNA microarray experiments. Anal. Gene Expr. Data 313–341.
Zhu, M.T., Feng, W.Y., Wang, B., Wang, T.C., Gu, Y.Q., Wang, M., Wang, Y., Ouyang, H., Zhao, Y.L., Chai, Z.F., 2008. Comparative study of pulmonary responses to nano- and submicron-sized ferric oxide in rats. Toxicology 247, 102–111.